Comparison of the TEP method for neutral particle transport in the plasma edge with the Monte Carlo method

2001 Nucl. Fusion 41 1003

(http://iopscience.iop.org/0029-5515/41/8/305)

Comparison of the TEP method for neutral particle transport in the plasma edge with the Monte Carlo method

R. Rubilar, W.M. Stacey, J. Mandrekas
Fusion Research Center, Georgia Institute of Technology,
Atlanta, Georgia, United States of America

Abstract. The transmission/escape probability (TEP) method for neutral particle transport has recently been introduced and implemented for the calculation of 2-D neutral atom transport in the edge plasma and divertor regions of tokamaks. The results of an evaluation of the accuracy of the approximations made in the calculation of the basic TEP transport parameters are summarized. Comparisons of the TEP and Monte Carlo calculations for model problems using tokamak experimental geometries and for the analysis of measured neutral densities in DIII-D are presented. The TEP calculations are found to agree rather well with Monte Carlo results, for the most part, but the need for a few extensions of the basic TEP transport methodology and for inclusion of molecular effects and a better wall reflection model in the existing code is suggested by the study.

1. Introduction

The presence of neutral atoms and molecules in the edge of a magnetically confined plasma plays an important role in the overall plasma performance. For instance, there are strong indications [1] that the onset of detachment is influenced by the neutral population in the divertor region. Recent reports [2] point out that edge neutrals have an important influence on the H mode transition in JT-60U. It has been reported recently that, in DIII-D continuous gas fuelled H mode discharges, MARFE onset was correlated with a sharp increase in neutral concentration in the plasma edge [3]. Therefore, it seems likely that an efficient and accurate computational method for neutral particle transport will contribute to a better understanding of many important physics effects in tokamak plasmas.

Neutral particle transport in the plasma edge is characterized by geometrical complexity, widely varying mean free paths (from millimetres to metres) and a wide plasma particle density variation (10^{17}–10^{21} m^{-3}) and range of gradient scale lengths (millimetres to metres). Most of the methods previously used to study neutral particles in plasmas are limited either by large computational times (Monte Carlo), inability to treat complex geometries, difficulty in treating widely varying mean free paths (differential transport methods such as diffusion theory or discrete ordinates) or lack of accuracy in some regimes (diffusion theory).

An interface current balance methodology has recently been developed to treat 1-D [4] and 2-D [5] neutral particle transport problems in the outer regions of a diverted tokamak plasma. In the transmission/escape probability (TEP) method [5] the computational domain is subdivided into a number of relatively large regions, transmission and escape probabilities are calculated for these regions using first flight integral transport methods, and then a balance is performed relating the partial currents, or directional fluxes, across the surfaces bounding these regions. In implementing this methodology, a number of approximations were made in order to simplify the treatment of the angular distribution of incident particles, the spatial distributions of collisions within a region, and the spatial distributions of plasma density and temperature within a region in the calculation of the basic transport probabilities; the accuracy of these basic approximations has been evaluated in a previous article [6], and this evaluation is summarized and extended somewhat here. However, the main purpose of this article is to present comparative calculations made with the TEP and Monte Carlo methods for more realistic experimental geometries. Included in this comparison is an analysis of a recent set of neutral density measurements in DIII-D.

The TEP methodology is summarized in Section 2. The effects of approximations in the calculation of the transport probabilities are investigated for a simple 2-D model problem in Section 3. Approximations in the treatment of the neutral energy

distribution are also discussed in Section 3. In Section 4, a comparison of TEP and Monte Carlo calculations for a DIII-D model is presented. Analysis of a recent DIII-D neutrals experiment is discussed in Section 5. Finally, the results of this article are summarized and recommendations are presented in Section 6.

2. TEP transport methodology

The TEP transport methodology in 2-D configurations is developed [5] by writing the partial current from region i into region j, J_{ij}, in the following form:

$$J_{ij} = \sum_{k}^{i} J_{ki} T_{0i}^{kj} + \sum_{k}^{i} \left(1 - \sum_{l}^{i} T_{0i}^{kl}\right) J_{ki} c_i P_i \Lambda_{ij} + s_i P_i \Lambda_{ij}^{s} \quad (1)$$

as illustrated schematically in Fig. 1. The first term represents the sum of the partial currents entering region i from all contiguous regions k, times the probability T_{0i}^{kj} that the particle is transmitted across region i uncollided to exit into region j. The second term represents the sum of the partial currents entering region i from all contiguous regions, times the probability that they have a collision in region i, times the probability c_i that the collision was a scattering or charge exchange event, times the total escape probability P_i that the particle (or its progeny) escapes region i after one or more scattering or charge exchange collisions, times the probability Λ_{ij} that the scattered particle escaping from region i goes into region j. The third term represents any internal source of particles in region i (e.g., recombination), times the escape probability P_i that the particle in region i escapes into region j, times the probability Λ_{ij}^{s} that the escaping source particle will enter region j.

Equation (1) is written for the partial currents in each direction across each interface in the problem, including reflective or vacuum (non-reflective) boundaries. The resulting set of interface current balance equations are then solved by standard linear algebra techniques.

The physics of the transport process is embedded in the transmission and escape probabilities. The first flight transmission probability T_{0i}^{kj} in 2-D planar geometry (i.e. with symmetry in the third dimension) for particles going from region k into region j across

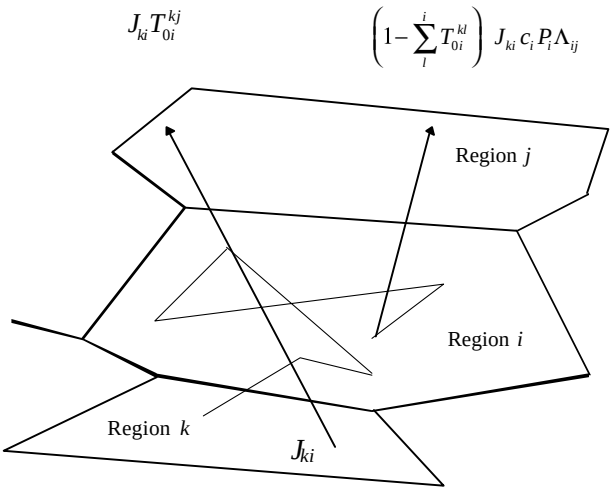

Figure 1. Transmission and escape probabilities (TEPs) schematic diagram in 2-D geometry.

region i can be defined in terms of Bickley functions Ki_n [6]

$$T_{0i}^{kj} = \frac{2}{\pi L_i} \int_{\xi_{ki}^{min}}^{\xi_{ki}^{max}} d\xi_{ki} \int_{\phi_j^{min}(\xi_{ki})}^{\phi_j^{max}(\xi_{ki})} \times d\phi_j \sin\phi_j Ki_3\left(l_i[\phi_j(\xi_{ki})]/\lambda_i\right) \quad (2)$$

where the co-ordinate ξ_{ki} is along the interface between regions k and i of length L_i, $\lambda_i = 1/\Sigma_i$ is the mean free path (the inverse of the macroscopic total cross-section) and l_i is the distance in the 2-D plane from a point ξ_{ki} on the entering surface to a point on the exiting surface, defined by $\phi_j(\xi_{ki})$, which is the angle made with respect to the surface between regions k and i by a line in the 2-D plane connecting the point ξ_{ki} on that surface with a point on the surface between regions i and j [6].

A similar expression can be used in defining the first flight escape probability P_{0i} [6]. However, it is more computationally efficient to calculate the first flight escape probability using a rational approximation of the form

$$P_{0i} = \frac{1}{X_i}\left[1 - \left(1 + \frac{X_i}{n}\right)^{-n}\right] \quad (3)$$

where the parameter $X_i \equiv 4V_i/\lambda_i S_i$ is defined in terms of the volume (area in 2-D) V_i, the surface area (circumference in 2-D) S_i and the mean free path λ_i of region i. This type of rational approximation for the escape probability was introduced by Wigner et al. [7], extended to cylindrical geometry by Sauer [8] and recently generalized by us [6].

The total escape probability from a region, P_i, can be constructed by summing the probability P_{0i} of

escaping after one collision, the probability $P_{0i}c_i(1-P_{0i})$ of a neutral particle 'surviving' the first collision and having a second collision and then escaping, the probability $P_{0i}[c_i(1-P_{0i})^2]$ of surviving the first two collisions and then escaping after the third collision, etc., to obtain $P_i = P_{0i}/[1-c_i(1-P_{0i})]$. Here c_i is the probability of a neutral particle emerging from a collision between a neutral particle and a plasma particle (i.e. the ratio of the charge exchange plus elastic scattering rates to the total reaction rate).

3. Test of transport methodology

3.1. Calculation of transmission and escape probabilities

We previously confirmed the accuracy of the algorithm of Eq. (2) used to calculate T_0 by comparison with Monte Carlo for a variety of region geometries and mean free paths [6]. The results were in excellent agreement for regions with uniform media and for regions with non-uniform density in which the average density was used to evaluate an effective mean free path for the region. For regions with a linear temperature distribution with gradient scale length L_T for which an effective mean free path was calculated from the average temperature, the errors in T_0 are shown in Table 1 for two values of the ratio $\Delta x/\lambda$ of the region dimension to the mean free path. Clearly the error scales as $\Delta x/\lambda$, but not with $\Delta x/L_T$. Note that the strong variation of the ionization cross-section over the interval 1–10 eV causes a somewhat larger error than occurs in the interval 10–100 eV for the same value of $\Delta x/L_T$, and that there is apparently a cancellation of errors over the temperature interval 1–100 eV.

Monte Carlo simulations performed on a number of geometries with different volume to surface ratios and different mean free paths confirmed that the first flight escape probability P_0 depended on only a single parameter, namely $X = 4V/\lambda S$ [6].

The Wigner rational approximation ($n = 1$) is known to underpredict P_0 for intermediate values of X, and the Sauer approximation ($n = 4.58$) was developed as an improvement for cylinders. We found [6], by fitting the results of Monte Carlo calculations, that a new rational approximation ($n = 2.09$) was very accurate for the calculation of P_0 in a variety of geometries. This improved rational approximation was superior to those suggested by Wigner ($n = 1$) for all geometries and Sauer ($n = 4.58$) for all geometries except cylindrical. The P_0 predicted by the new rational approximation was within 5% (for both uniform and non-uniform regions) of the Monte Carlo calculation for all geometries tested except cylindrical, for which Sauer's approximation ($n = 4.58$) was superior.

Table 1. Error in transmission coefficient caused by using an average mean free path over a region with temperature gradient

ΔT (eV)	100–50	100–10	100–1	10–1
$\Delta x/L_T$	0.67	1.63	2.00	1.63
Error (%) for $\Delta x/\lambda = 2.2$	3.23	2.94	−0.37	4.78
Error (%) for $\Delta x/\lambda = 0.22$	0.32	0.24	−0.19	0.66

Comparisons [6] with Monte Carlo calculations for square regions with linear temperature or density variations provided a test of the accuracy of the assumption that the rational approximation can be used to calculate the total escape probability P for a non-uniform region by simply using an effective mean free path calculated with the average plasma density and temperature in the region. In non-uniform temperature problems with $\Delta x/\lambda_{av} = 2.2$, the errors in the rational approximation for P were about 2% for temperature variations with $\Delta x/L_T = 1.6$ over the intervals 1–10 eV and 10–100 eV. In non-uniform density problems, the errors in the rational approximation for P were 3.5% for $\Delta x/\lambda_{av} = 3.4$ and $\Delta x/L_n = 0.67$ and 0.5% for $\Delta x/\lambda_{av} = 2.3$ and $\Delta x/L_n = 1.8$.

3.2. Transport in 2-D multiregion model problems

The purpose of this section is to report an investigation of the accuracy of the TEP methodology for relatively simple 2-D model problems. The model problems were chosen to be sensitive to a particular aspect of the calculation. The model used was a square region subdivided into nine identical cells (Fig. 2). The dimension of each cell was $\Delta x = 0.30$ m. The model problem had uniform plasma density and temperature and vacuum boundary conditions (i.e. no recycling at the boundary) on the four external surfaces. No molecular processes were included in the calculations. An incident flux of particles entered the right surface of cell 6 (Fig. 2). The same cell arrangement and plasma parameters were used in both the Monte Carlo neutral transport

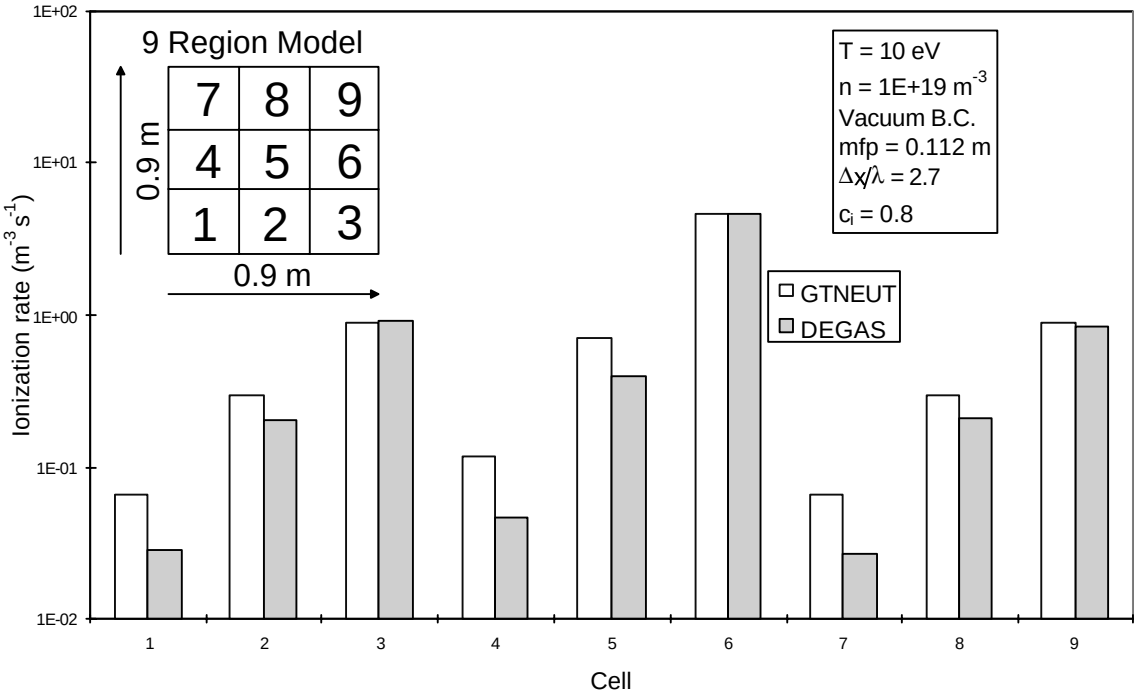

Figure 2. Ionization rate density for a nine uniform region model with $\Delta x/\lambda = 2.7$, vacuum boundary conditions and $c_i = 0.8$.

code DEGAS [9] and the TEP code GTNEUT [5]. In GTNEUT, the incident neutrals had a Maxwellian energy distribution at the local ion temperature of region 6. In the DEGAS calculation, the incident neutrals had a Maxwellian energy distribution at the ion temperature of region 6 and a cosine angular distribution. In the GTNEUT calculation, the incident particles were not distributed in energy but the reaction rates were averaged over Maxwellian distributions of the neutrals (assumed to be the same as that of the ions) and ions or electrons, and the angular distribution of the incident neutrals was isotropic.

We have previously identified [6] two approximations that could potentially lead to inaccuracies in the TEP calculations when $\Delta x/\lambda$ is much greater or much less than unity. The calculation of the first flight transmission coefficient T_0 in the TEP method is based on the assumption of an isotropic angular distribution in the incident hemisphere at each of the interfaces; this assumption is questionable for $\Delta x/\lambda \ll 1$. The calculation of the first flight escape probability is based on the assumption of a uniformly distributed collision source within a region; this assumption is questionable for $\Delta x/\lambda \gg 1$. Furthermore, the fraction Λ_{ij} escaping from region i into region j is presently calculated as the ratio of the area of the interface between regions i and j to the total area of the surfaces bounding region i; which is questionable for $\Delta x/\lambda \gg 1$.

It was found [6] in 1-D model problems with a strong directional flow of particles that:

(a) The isotropization assumption made in calculating T_0 introduced an underprediction of penetration error which increased with decreasing $\Delta x/\lambda$ in the region (i.e. with increasing probability that an incident particle is transmitted across a region without a collision);

(b) The internal distribution of the first collision source decreased away from the incident surface, resulting in a larger probability of escape of collided particles back across the incident surface than forward across the opposite surface, so that the assumption of the same escape probability in both the forward and backward directions leads to an overprediction of penetration — this error increases as $\Delta x/\lambda$ increases (i.e. as the first collision source distribution becomes more peaked towards the incident surface).

Both errors were found to compound with the number of interfaces (regions) in the problem. Thus, in problems with a strong directional flow of particles

away from a source, one would expect an underprediction of penetration for $\Delta x/\lambda < 1$ and an overprediction of penetration for $\Delta x/\lambda > 1$. We further investigate these two potential sources of error in this section.

In the first case considered, the plasma temperature and density were uniform ($T = 10$ eV, $n = 1 \times 10^{19}$ m^{-3}). The average number of neutrals emerging from a collision,

$$c_i = \frac{\langle \sigma v \rangle_{CX} + \langle \sigma v \rangle_{el}}{\langle \sigma v \rangle_{CX} + \langle \sigma v \rangle_{el} + \langle \sigma v \rangle_{ion}} \tag{4}$$

was 0.8.

The mean free path of the neutrals was $\lambda = 0.112$ m, which was smaller than the dimension of each cell (i.e. $\Delta x/\lambda = 2.7$). For $\Delta x/\lambda \gg 1$, the directional escape probability error should be dominant over the isotropization error, resulting in a net overprediction of penetration. The first collision source distribution was peaked towards the incident surface. This caused the true escape probability across the incident surface (from cell 6 to the right) to be greater than the escape probability across the opposite surface (from cell 6 into 5). The escape directionality error made in assuming that $\Lambda = 0.25$ for all surfaces would cause the overprediction of particles emerging from the opposite surface of region 6 into region 5. In other words, penetration should be overpredicted.

Thus, the particle ionization rate predicted by TEP (GTNEUT) was expected to be greater than that predicted by the Monte Carlo method (DEGAS) in the cells further away from the source (i.e. cells 1, 4, 7, 2, 5 and 8) because of this escape directionality error, and indeed it was. With reference to Fig. 2, the results for cell 6 were in excellent agreement with the Monte Carlo ones because the total escape probability (i.e. the total number of particles leaving the cell) was predicted correctly. The results in cells 3 and 9 were also in good agreement because the up–down directional escape probability from cell 6 across the lateral surfaces into regions 3 and 9 was not sensitive to the left–right distribution of the first collision source rate in cell 6.

In the second case considered, the ion density was reduced to 1×10^{18} m^{-3}. The temperature and c_i were identical to those in the first case. The mean free path of the neutrals was $\lambda = 1.12$ m so that $\Delta x/\lambda = 0.26$. When the dimension of the region is smaller than the mean free path of the particle, the uncollided fluxes become more forward peaked in angular distribution while traversing the region. Thus, the effect of isotropizing (assuming an isotropic incident particle distribution for calculating T_0) at each surface introduces an isotropization error at each interface. This isotropization error causes an underprediction of penetration and would be expected to dominate the directional escape probability error for $\Delta x/\lambda \ll 1$, which would cause the ionization rate predicted by TEP (GTNEUT) to be less than that predicted by DEGAS in the cells away from the source (i.e. cells 1, 2, 4, 5, 7 and 8). This result can be observed in Fig. 3. It is also noteworthy that the results in cells 3, 6 and 9 were in excellent agreement with the Monte Carlo ones. The reason for this agreement is that the left–right isotropization error did not affect the up–down transmission probabilities across cell 6 into cells 3 and 9.

In the third case considered, the ion density was equal to 3.7×10^{18} m^{-3}. The temperature and c_i were identical to those in the previous cases. The mean free path of the neutrals was $\lambda = 0.30$ m, the same as the dimension of each region. We observed previously [6] that when the mean free path is equal to the characteristic dimension of the region (i.e. $\Delta x/\lambda = 1$), the isotropization and directional escape probability errors tended to balance each other almost exactly. Thus, good agreement with the Monte Carlo method was expected, and this was in fact observed in all regions (Fig. 4). Similar agreement was observed in another problem with $\Delta x/\lambda = 1$, but with a charge exchange plus elastic scattering probability $c_i = 0.6$. However, the value of $\Delta x/\lambda$ at which exact compensation is found between the isotropization and directional escape probability errors depends on the number of regions into which the computational domain is divided (i.e. the number of interfaces at which the errors are made). The value of $\Delta x/\lambda$ at which the two errors exactly compensate generally decreases with an increasing number of interfaces in the direction of penetration. These results suggest the use of cells with $\Delta x/\lambda \sim O(1)$ in regions with a large plasma background. Since the TEP method becomes exact for single regions with $\Delta x/\lambda \to 0$, the near vacuum plenum regions can be large. Planned extensions to the TEP methodology to reduce or eliminate the isotropization and directional escape probability errors are discussed in Section 6.

A simple timing study was performed on a series of 'square' problems with vacuum boundary conditions of the type discussed above, but with a progressively increasing number of regions N. The GTNEUT CPU time increases with the number of regions. This increase is mostly due to the additional computations

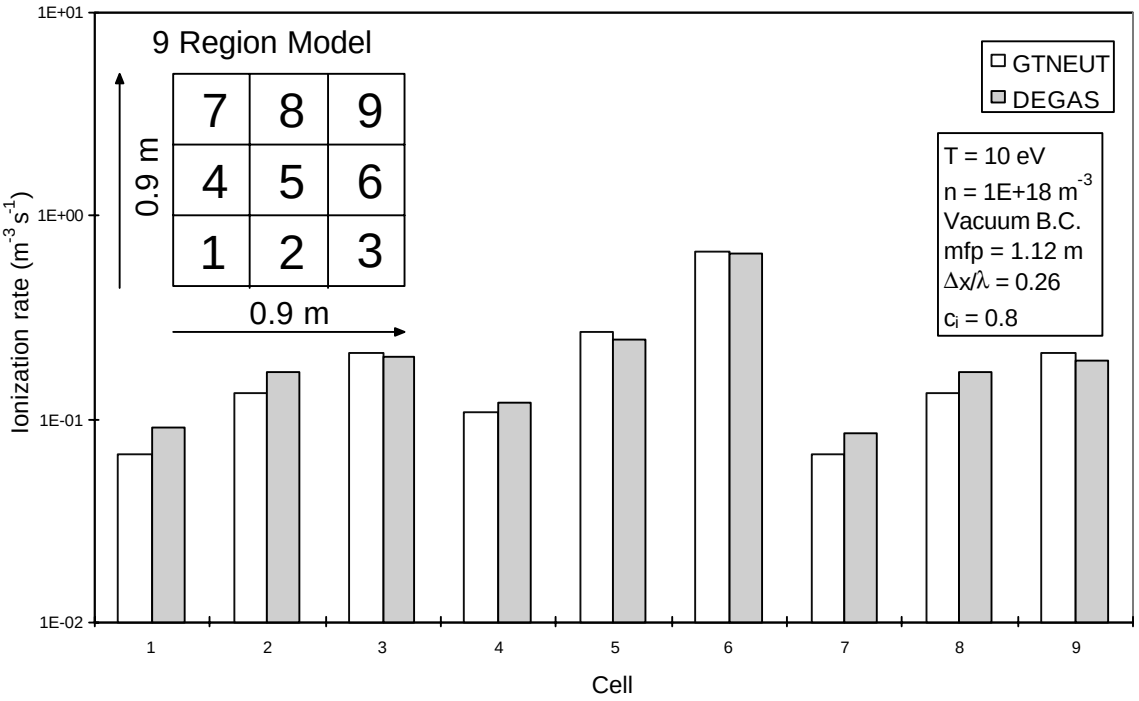

Figure 3. Ionization rate density for a nine uniform region model with $\Delta x/\lambda = 0.26$, vacuum boundary conditions and $c_i = 0.8$.

required for the evaluation of the extra transmission coefficients for the increased number of interfaces that are added to the problem when the number of regions increases. For this 2-D model problem, the GTNEUT CPU time was found to scale as $\sim N^k$, where N is the number of regions and $k \approx 2$. The CPU time does not depend on the background plasma properties.

A similar CPU time dependence was found for the DEGAS code for the same series of problems. In order to keep the Monte Carlo error the same as the number of cells increased, we had to increase the number of particle histories in the DEGAS simulation. The DEGAS CPU time was about a 100 times longer than that for GTNEUT, but we emphasize here that in our comparisons with Monte Carlo, the original DEGAS code was used. A new faster version of DEGAS, DEGAS 2, is currently available that is about a factor of 10 faster than the original code for most practical problems [10].

3.3. Neutral energy distribution

Both the transmission and escape probabilities depend on the mean free path of the neutral particles, which is defined in terms of a reaction rate $\langle\sigma\nu\rangle$, averaged over the neutral and plasma ion (for charge exchange and elastic scattering) or electron (for ionization) distribution functions, and an average neutral speed v_n. When the distribution functions are Maxwellians with temperatures T_n and $T_{i,e}$, the mean free path can be written as

$$\lambda \equiv \Sigma^{-1} = \frac{v_n}{n_e\langle\sigma\nu(T_n,T_e)\rangle_{ion}+n_i\langle\sigma\nu(T_n,T_i)\rangle_{CX}+n_i\langle\sigma\nu(T_n,T_i)\rangle_{el}} \quad (5)$$

where $v_n = (2T_n/m_n)^{1/2}$, with m_n being the neutral particle mass.

It is important to keep in mind that the total reaction rate $\langle\sigma\nu\rangle$ is a function of ion and electron temperature and electron density (ionization rate), and that the mean free path is proportional to the square root of the energy of the neutral. Neutrals can either gain or lose energy through successive scattering or charge exchange with energetic ions. A realistic assumption might be that after a scattering or charge exchange collision event, the neutrals entering a region attain the local ion energy distribution, which means $T_n = T_i$. This 'local ion temperature' approximation is used in the GTNEUT code.

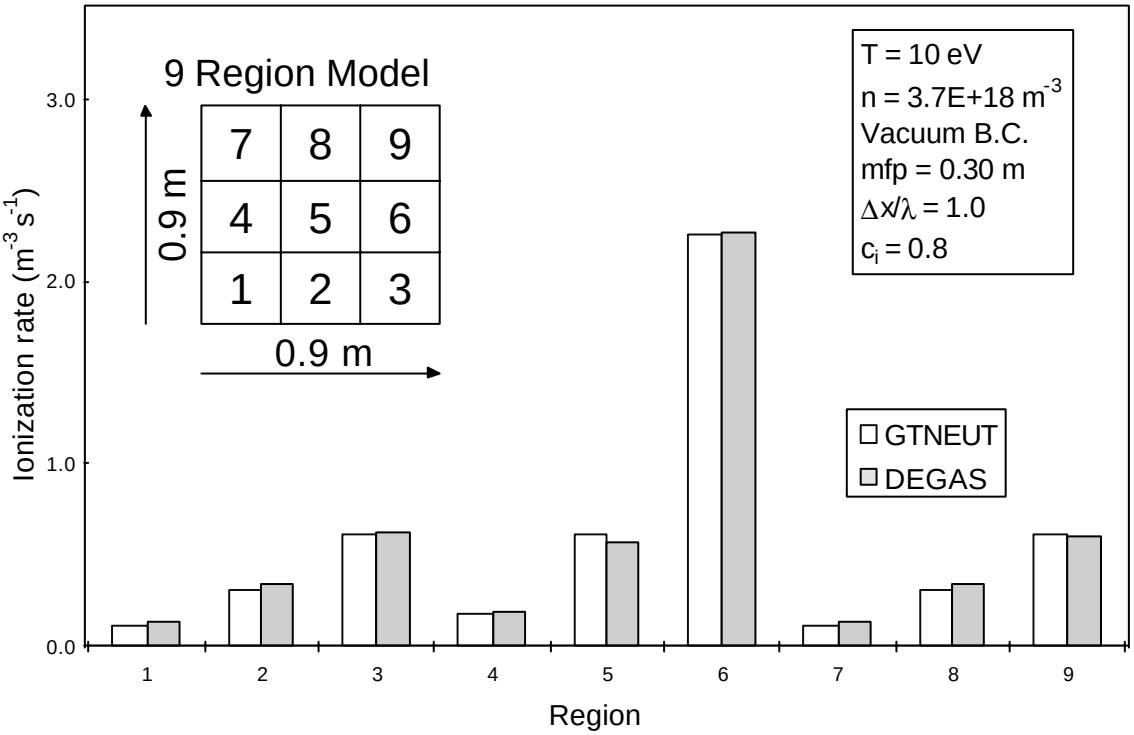

Figure 4. Ionization rate density for a nine uniform region model with $\Delta x/\lambda = 1.0$, vacuum boundary conditions and $c_i = 0.8$.

We evaluated the accuracy of the local ion temperature approximation in a non-uniform 1-D multi-region problem. The model consisted of a slab with a linear temperature distribution and uniform density, subdivided into ten regions. Vacuum boundary conditions were imposed on the left and right hand surfaces. The plasma temperature varied from 10 eV on the left hand boundary to 100 eV on the right hand boundary. The dimension Δx of each region was set equal to the mean free path of the neutral in the region, thus creating the condition for which the isotropization and escape directionality errors almost exactly compensate each other (i.e. $\Delta x/\lambda = 1$), so that any differences in the TEP (GTNEUT) and continuous energy Monte Carlo (DEGAS) calculation can be attributed to the local ion temperature approximation. The charge exchange and scattering fraction c_i in this model problem varied between 0.78 in the leftmost region to 0.59 in the rightmost region.

In both DEGAS and GTNEUT, a neutral gas source with a Maxwellian distribution (T_n = 10 eV) was present on the left hand boundary. The GTNEUT calculation assumed that the neutrals going from region 1 to region 2 acquired a Maxwellian energy distribution at the local ion temperature of region 2, i.e. $E_n = T_{i2}$. DEGAS, on the other hand, calculated a continuous energy distribution of neutrals.

The results of the GTNEUT and DEGAS predictions for the ionization rate can be seen in Fig. 5. The predicted results of GTNEUT with the local ion temperature model and DEGAS showed excellent agreement. This figure also shows a GTNEUT prediction in which the neutral energy was held constant at 10 eV (crosses), and showed large discrepancies with Monte Carlo results, particularly at deep penetration.

We tentatively conclude that the local ion temperature approximation is adequate in regions where the mean free path is comparable to the scale length of the temperature variation. However, we might expect this local ion temperature assumption to break down in regions where the mean free path is greater than the scale length of the temperature variation or near material surfaces where the energy of the reflected neutrals and ions depends on the material and on other external considerations such as sheath acceleration.

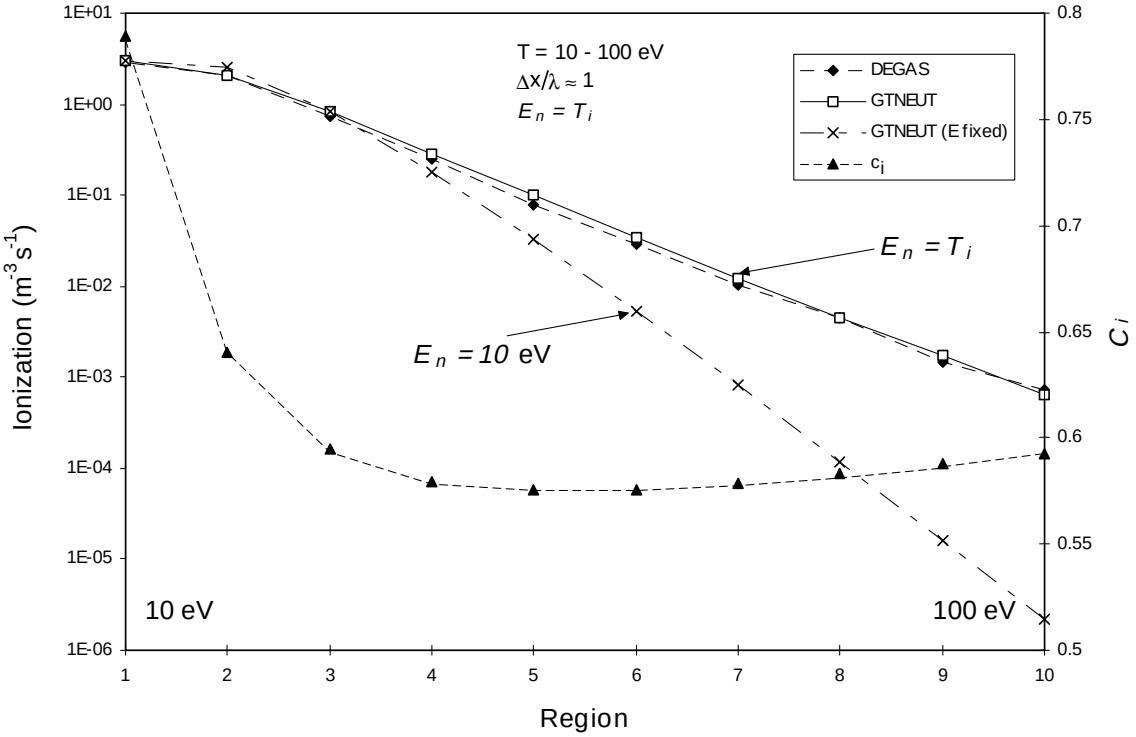

Figure 5. Ionization rate in a problem with linearly varying temperature. Neutral energy equal to the local ion temperature (closed diamonds), $E_n = T_i$. Fixed neutral energy (crosses), $E_n = 10$ eV.

4. Experimental model problems

Having tested the accuracy of the various approximations made in implementing the TEP methodology on simple model problems chosen to be sensitive to the individual approximations (Refs [6, 11] and Section 3), we now turn to testing the accuracy of the TEP method (with the approximations discussed in the previous sections) for model problems that are more representative of experimental configurations. We have carried out GTNEUT and DEGAS comparison calculations for model problems based on the full geometry of the DIII-D and Alcator C-Mod tokamaks and of the ITER EDA conceptual design [11]. This section presents the results of the DIII-D divertor model problem comparison.

4.1. DIII-D model problem

The geometry of the plasma, SOL, divertor and plenum regions for the DIII-D model problem is shown in Fig. 6. This DIII-D geometric model was represented in GTNEUT with 48 cells. We note that a much finer 'grid structure' is normally used in Monte Carlo neutrals calculations because of the finer 'grid structure' used in the edge plasma fluids codes. However, our purpose here is to extend our comparison of the TEP and Monte Carlo calculations to more complex geometries representative of the plasma edge, not to model the spatial detail of the plasma edge. The low density regions near the wall were represented by the cells with odd numbers between 1 and 41. The SOL region just outside the separatrix was represented by the cells labelled with even numbers between 2 and 42. The inner divertor plate was represented by the wall segment 52. Particles were recycled in front of the inner divertor plate in cell 2. The wall segment 75 represented the outer divertor plate. The corresponding recycling cell was 43. The low density private flux region was represented by cells 44 to 48. The background plasma temperatures and densities used in this simulation were representative of DIII-D plasma conditions: 200 eV and 10^{20} m^{-3} for edge plasma regions inside the LCFS; 10 eV and 5×10^{18} m^{-3} for odd numbered plenum regions between 1 and 41; 100 eV and 10^{19} m^{-3} for even numbered divertor–SOL plasma regions between 8 and 40; 10 eV and 10^{20} m^{-3} for recycling regions 2 and 43; 50 eV and 5×10^{19} m^{-3} for divertor plasma regions 4, 6 and 42;

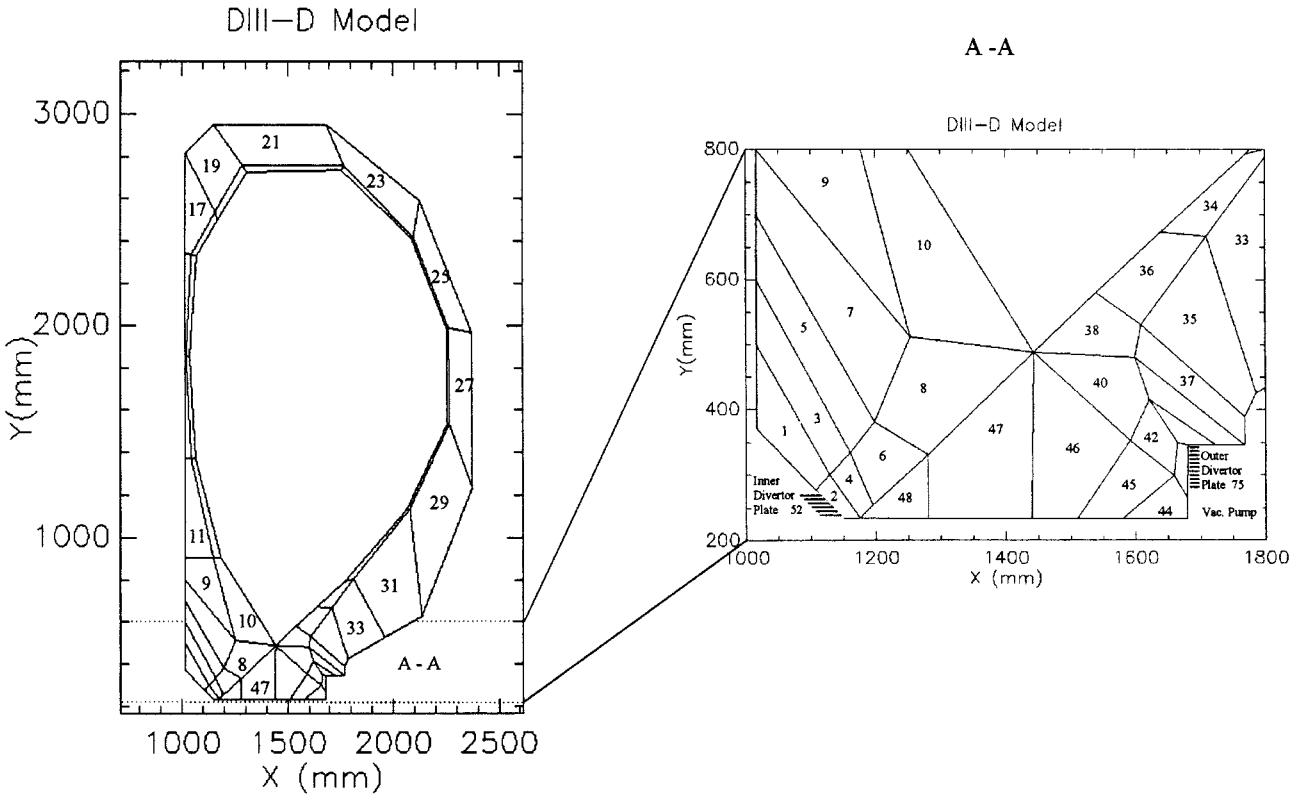

Figure 6. DIII-D model problem geometry.

Table 2. Relation between cell dimension and mean free path for selected cells in the DIII-D model problem

Cell	Δx (cm)	λ (cm)	$\Delta x/\lambda$
2	3.2	1.1	2.9
4	3.6	2.2	1.64
6	9.0	2.2	4.1
8	18.0	12.7	1.42
40	13.4	12.7	1.05
42	8.0	2.2	3.63
43	2.5	1.1	2.36
44–48	6.7–18.0	22.4	0.3–0.8

and 10 eV and 5×10^{18} m^{-3} for private flux regions 44–48.

The relation between the cell dimension Δx and the mean free path λ for some selected cells of Fig. 6 is shown in Table 2. In this case, the characteristic cell dimension is taken as the dimension in the general direction of neutral flow from the recycling source at the divertor plate towards the core plasma.

The ion flux was reflected isotropically as neutral atoms into cells 2 and 43 with an energy $E_n = T_i$, where T_i is the ion temperature just in front of the divertor plate (i.e. in cells 2 and 43) and then transported into the adjacent cells. The GTNEUT calculation assumed that the neutrals reflected from the divertor plate, those reflected from the wall and those transported into a given cell acquired (via charge exchange and scattering) a Maxwellian energy distribution with the local ion temperature of the cell in question.

For comparison, a benchmark DEGAS simulation was carried out with the same cell arrangements and plasma parameters. In the Monte Carlo calculation, ions selected from a Maxwellian ion distribution characterized by the temperature in the region next to the material surface were specularly reflected ('mirror' wall boundary condition) as neutral atoms with the incident ion energy. (This mirror condition is the only DEGAS option for reflecting atoms at the incident ion energy, the assumption used in GTNEUT.) The recycling of the incident ion flux from the divertor plates was approximated by a puff of neutrals with an energy corresponding to a Maxwellian with the local ion temperature of the region in front of the divertor plates (i.e. cells 2 and 43). DEGAS calculates the neutral energy distribution in all regions.

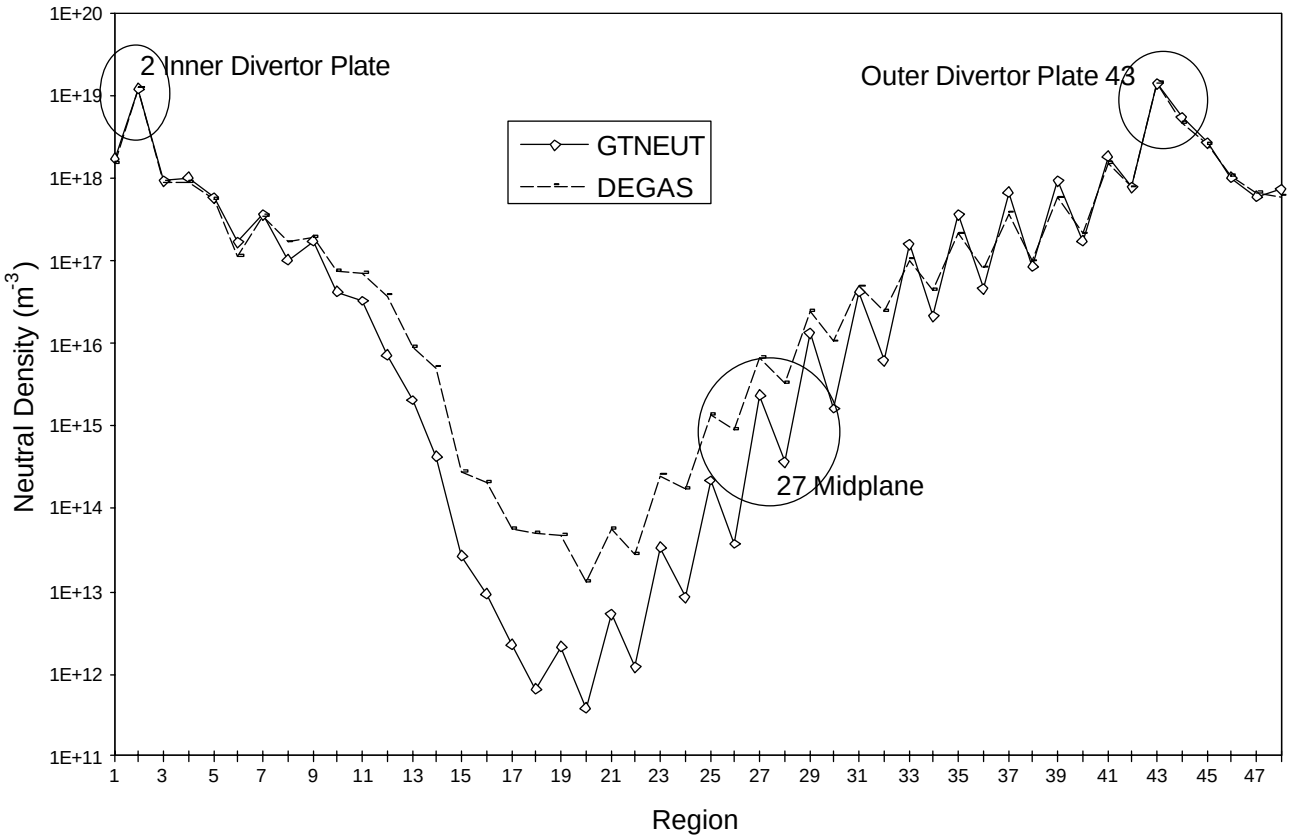

Figure 7. Neutral particle density calculated for the DIII-D model problem.

4.2. Comparison of the GTNEUT and DEGAS calculations for the DIII-D model problem

The results of the GTNEUT and DEGAS simulations for the neutral particle density are shown in Fig. 7 (the oscillating appearance is an artefact of the cell numbering system).

The results of GTNEUT and DEGAS agreed quite well in the vicinity of the recycling source (i.e. cells 1–5 and 40–43) and in the divertor region, and reasonably well in the lower part of the model, where the neutral density was significant. For example, the GTNEUT and DEGAS compression ratios at the X point n_{DIV}/n_{Xpt}, which were of the order of 10^2, were in excellent agreement. Larger differences began to be observed in cells 11 and 37, where the results for the neutral density differed by a factor of approximately two.

It is more difficult to reconcile the differences between the two calculations in terms of the isotropization and directional escape probability errors discussed in Section 3 because the geometry is more complex. However, we can gain some insight by considering divertor plasma regions 8 and 40, in which GTNEUT slightly underpredicts DEGAS. The neutrals reaching these regions either:

(a) Stream directly up the plasma channel from the recycling source at the divertor plate, passing through regions 2, 4 and 6 to get to region 8 or passing through regions 43 and 42 to get to region 40;
(b) Stream across the private flux regions (44–48) from the recycling sources;
(c) Stream across the lower plenum regions (1, 3, 5, 7) and (39, 41) on the outboard side.

The divertor plasma regions have $\Delta x/\lambda > 1$, implying that the neutral concentrations in regions 8 and 40 from path 1 should be overpredicted due to the directional escape probability error. The private flux (and lower plenum) regions have $\Delta x/\lambda < 1$, implying that the neutral concentrations in regions 8 and 40 from path 2 (and 3) would be underpredicted due to the isotropization error. The relatively good agreement between GTNEUT and DEGAS in regions 8

Table 3. CPU* time (s) for tokamak problems

DIII-D		C-Mod		ITER-EDA	
GTNEUT	DEGAS	GTNEUT	DEGAS	GTNEUT	DEGAS
18	12784	35	70542	10	2983

* CRAY J90.

and 40 suggests that these two types of error compensate in the prediction of the neutral concentration in the divertor plasma channel near the X point in this model problem.

There were larger discrepancies between the results of the two codes in cells 12–36 in the upper region of the problem. It is believed that differences in the treatment of the reflective boundary conditions at the wall and edge–core interface in the two codes were partly responsible for these differences in the upper regions.

However, the differences between DEGAS and GTNEUT can be partially explained also by the statistical error in the Monte Carlo calculation. The DEGAS calculation was carried out with 500 000 histories, and the statistical errors were less than 1% for cells 1–10 (in or near the inner divertor region) and for cells 37–48 (in or near the outer divertor region). The error bars fluctuated from 12 to 40% in cells located between the midplane and the upper stagnation point, i.e. regions 14–27. In these upper cells GTNEUT predicted an attenuation, relative to the neutral density at the divertor plate, varying from of the order of 10^5 at the midplane to 10^8 at the upper stagnation point. The corresponding DEGAS attenuation was 10^4–10^6.

Similar calculations were performed for the C-Mod and ITER model problems (see Ref. [11] for a discussion of these calculations). The agreement between GTNEUT and DEGAS was similar to that discussed above for the DIII-D model problem (i.e. good in all cells where the neutral density had not been attenuated by more than 10^3–10^4 with respect to the divertor plate).

The time required to carry out the GTNEUT calculations for the three tokamak models is summarized in Table 3. The Monte Carlo (DEGAS) time reported here is for the number of histories required to reduce the statistical error in cells in the vicinity of the divertor plate (including cells in the divertor throat) to less than 10%. We note again that the newer version of the DEGAS Monte Carlo code (DEGAS 2) [10] is faster (by a factor of at least 10) than the version used in this analysis.

5. Analysis of DIII-D neutral measurements

The purpose of this section is to compare the neutral density, as predicted by the TEP based code GTNEUT, with both a recent measurement of the neutral density near the X point in the DIII-D tokamak and a plasma fluid/Monte Carlo (B2.5/DEGAS) neutrals calculation of that experiment [12].

The experimental procedure [12] consisted of measuring the D_α light emission in the lower divertor by means of a tangentially viewing charge injection device (CID) video camera (TTV). The image obtained was later used to generate a poloidal D_α light distribution. The electron temperature and density were measured at the divertor Thomson scattering locations. The neutral density was then calculated by using the relation

$$I_{D_\alpha} = n_e n_0 \langle \sigma \nu_e(T_e, n_e) \rangle_{exc} \tag{6}$$

where the quantities I_{D_α}, n_e and $\langle \sigma \nu_e(T_e, n_e) \rangle_{exc}$ represent the intensity of the TTV, the electron density measured by divertor Thomson scattering (DTS), and the electron excitation rate coefficient, respectively. During an L mode discharge (No. 96740) measurements were taken for the plasma located at several X point heights (6.9–13.8 cm) above the floor.

A 2-D model based on an iterated solution of a plasma fluid (B2.5) and a Monte Carlo (DEGAS) neutrals code was used by Colchin et al. [12] to predict the experimental measurements. The geometry for the 2-D GTNEUT model was based on this same DEGAS model. The model is depicted in Fig. 8. In the GTNEUT calculation, it was assumed that neutrals acquired an energy corresponding to a Maxwellian with the local ion temperature of the regions in question. DEGAS, on the other hand, calculated a continuous energy distribution in each region. The geometric model consisted of 190 cells, chosen to represent as accurately as possible the locations of the divertor plate, the X point, SOL and plasma core. The X point was located at

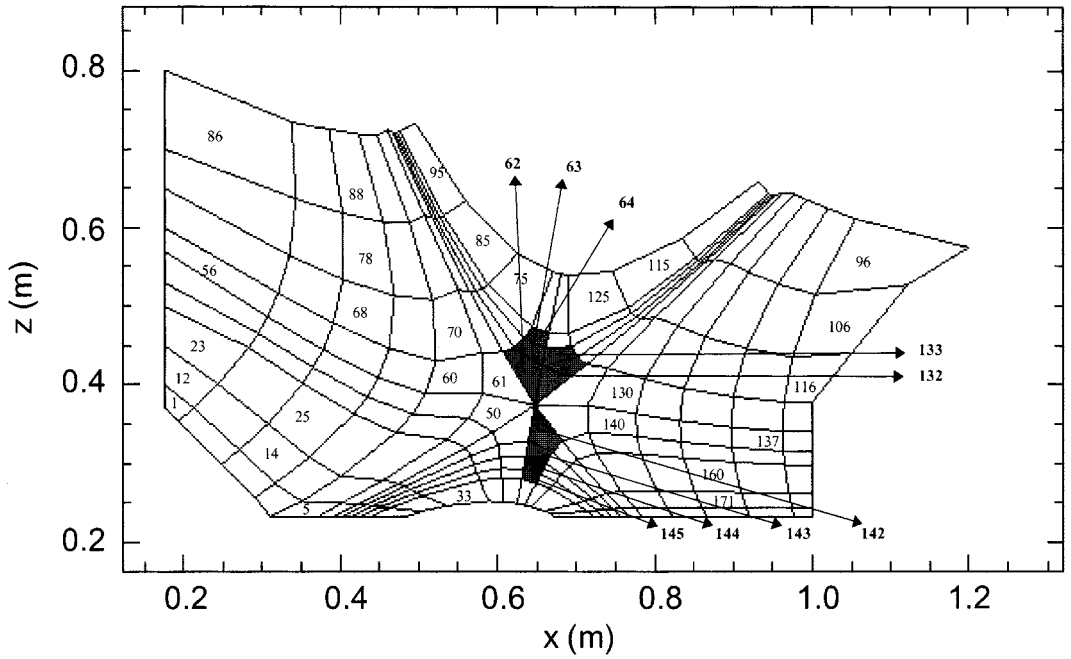

Figure 8. Neutral atom transport model for the DIII-D plasma experiment.

13.8 cm above the divertor floor. The shaded cells in Fig. 8 represent the location at which the measurements were taken. The plasma background temperature, density and recycling neutral source used in GTNEUT were the same as those used in the DEGAS calculation and were taken from the converged B2.5/DEGAS calculation. Table 4 summarizes these parameters for a few selective cells; again, the cell dimension is in the general direction of neutral flow from the recycling source at the divertor plate towards the plasma core.

The neutral densities predicted by GTNEUT and DEGAS and the measured neutral densities [12] are shown in Fig. 9. The experimental error bars are also shown [13]. The results obtained with the DEGAS calculation are in very good agreement with the measured neutral densities above the X point in the plasma edge inside the separatrix. The DEGAS results were not as good for those cells below the X point. The discrepancies between the B2.5/DEGAS calculation and the experimental results were attributed [12] to two factors:

Table 4. Plasma background information for DIII-D neutral experiment models

Cell	T_e (eV)	T_i (eV)	n_i (10^{19} m^{-3})	Δx (cm)	λ (cm)	$\Delta x/\lambda$
33	1.6	2.3	0.046	3.1	241	0.13
50	6.8	13.3	1.52	5.1	8.9	0.57
61	19	35	1.29	5.6	9.5	0.59
62	52	63	3.19	4.7	3.6	1.3
63	66	96	1.67	2.9	7.7	0.38
64	75	121	1.40	2.3	9.8	0.24
132	61	137	1.20	4.9	12.1	0.41
133	69	146	1.13	2.9	13.0	0.22
142	16	27	0.374	3.9	32.3	0.12
143	10	22	0.168	2.4	80.8	0.03
144	6	12	0.129	2.0	106.2	0.019
145	3	6	0.109	1.7	118.7	0.014

(a) The fluid code's inaccurate representation of the plasma parameters in the region below the X point,
(b) The neglect of the molecular contribution to the total intensity of the D_α light emission in evaluating the measured neutral density contributions to the D_α light emission.

The DEGAS calculation treated the recycling of a fraction of the neutrals as molecules.

The GTNEUT calculation, which did not include molecular recycling, agreed fairly well with the experiment and with DEGAS in the private flux region. However, for cells above the X point, the GTNEUT code overpredicted both the experimental measurements and the predicted DEGAS values by about a factor of two.

5.1. Monte Carlo and GTNEUT modelling differences

GTNEUT obtained comparable, even somewhat better, agreement with the experiment in the private flux region than DEGAS. We note that the GTNEUT calculation did not include molecular or recombination effects, whereas both were included in the B2.5/DEGAS calculation and are probably important in some regions next to the recycling surfaces. However, since the same converged B2.5 code calculation of the background plasma was used for both the GTNEUT and DEGAS calculations, the influence of molecular and recombination effects on the background plasma is accounted for in both calculations. Furthermore, the D_α emission from any excited atoms produced by molecular dissociation was neglected in interpreting the experimental data. These differences in treating molecular and recombination effects could be a possible source of the differences in calculated and measured neutral densities.

However, in the core region above the X point, where molecular effects are unimportant, there was at least a factor of two difference between the DEGAS and GTNEUT calculations. At least seven possible causes could account for this disagreement:

(a) Different treatments of geometry in DEGAS (toroidal) and in GTNEUT (cylindrical),
(b) Different treatments of molecules and of the density dependence of ionization cross-sections in DEGAS (included) and in GTNEUT (omitted),
(c) Different treatments of the wall boundary angular reflection condition in DEGAS and GTNEUT,
(d) Different treatments of the energy of recycling particles from the wall in DEGAS and GTNEUT,
(e) Inadequate treatment of the directional escape probability Λ in GTNEUT,
(f) Inaccurate description of the flux angular distributions at the interfaces in GTNEUT,
(g) The approximation in GTNEUT that the neutral energy distribution is a Maxwellian with the local ion temperature.

Again, the geometrical complexity, and now the further complexity of additional physical processes, makes it difficult to determine the probable effect of the isotropization and directional collision probability errors (items (e) and (f) above) discussed for the simpler model problem in Section 3, but we can make the same sort of qualitative analysis given for the DIII-D model problem in Section 4. To reach region 63 inside the separatrix above the X point, particles recycling from the inner divertor strike region (on the left in Fig. 8) can:

(a) Diffuse up the inner divertor plasma channel through regions 50 and 61 (and others) and then across the separatrix and through region 62;
(b) Flow up the divertor plenum region and through regions 60, 61 and 62;
(c) Flow through the private flux regions (33 and others) across the separatrix near the X point and then across region 62.

In all of these regions, except region 62, $\Delta x/\lambda < 1$ so that we might expect the isotropization error to dominate and produce an underprediction of the neutral density in region 63. Regions 63 and 133 are averaged to produce the prediction of neutral density shown at about 17.5 cm above the floor in Fig. 9, and this prediction is above both the experiment and the DEGAS predictions, so that one or more of the other possibilities listed above must be causing the disagreement.

The first four possibilities listed above are 'non-transport' effects due to differences in modelling the experiment, the atomic/molecular data or the wall reflection condition between DEGAS and GTNEUT. We found that (i) the differences in geometric representation were unimportant, but that (ii) the inclusion of molecules and (iii) the different treatment of wall reflection conditions could account

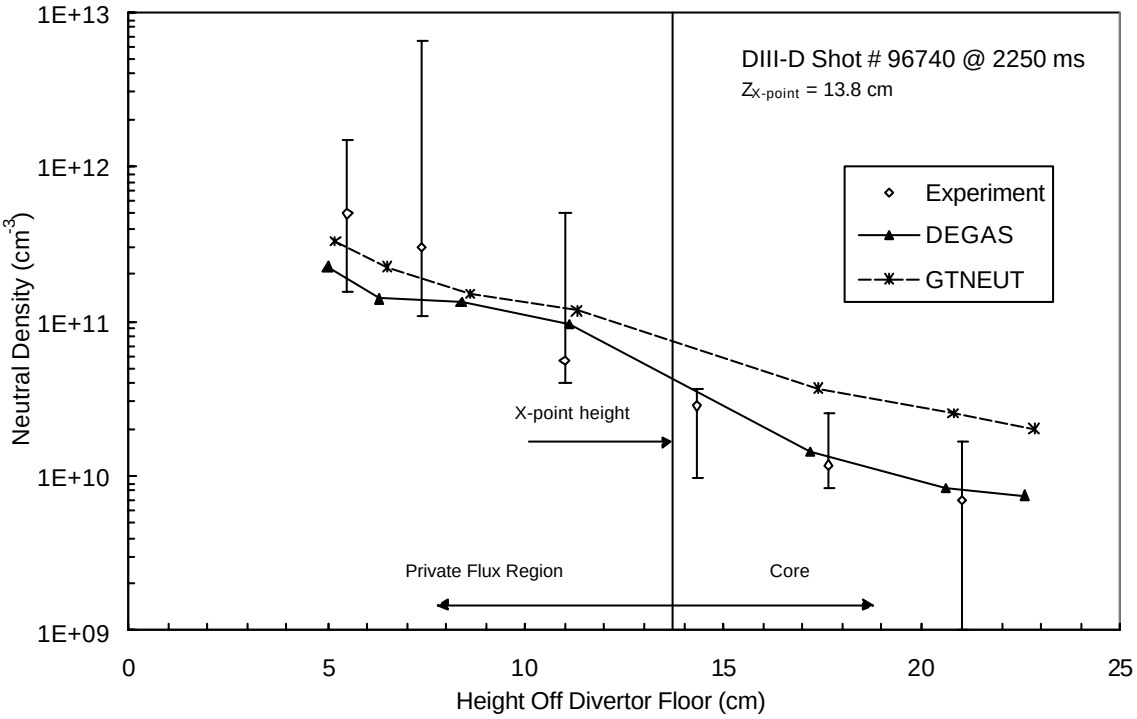

Figure 9. Neutral density as a function of height above the divertor floor (molecular effects and density dependent ionization rates included in DEGAS, but not in GTNEUT).

for the observed differences between GTNEUT and DEGAS, as will now be discussed.

5.1.1. Molecular and ionization cross-section differences

The GTNEUT calculation did not include molecules, but rather assumed that all incident ions and neutrals were reflected as atoms. Furthermore, the GTNEUT calculation treated the electron impact ionization rate, $\langle \sigma v \rangle_{ion}$, as independent of density. Since the original DEGAS calculation shown in Fig. 9 included molecules and a density dependent $\langle \sigma v \rangle_{ion}$, we ran two additional Monte Carlo simulations in order to evaluate the effect of these differences in molecular and atomic data treatments on the comparison of the GTNEUT and DEGAS transport calculations shown in Fig. 9. In the first run, the Monte Carlo simulation was performed without molecules, but with the electron impact ionization rate $\langle \sigma v \rangle_{ion}$ dependent on density. In the second run, the Monte Carlo simulation was carried out without molecules and without a $\langle \sigma v \rangle_{ion}$ dependence on density. Comparison of the two DEGAS calculations which differed only by the treatment of the density dependence of $\langle \sigma v \rangle_{ion}$ indicated that this is a relatively small effect, albeit one which in small part accounts for the differences between the GTNEUT and DEGAS calculations shown in Fig. 9.

Comparison of the two DEGAS calculations which differed only by the inclusion of molecules indicated that the inclusion of molecules is quite important (as previously noted in Refs [14, 15]), particularly in the private flux region below the X point. Not including molecules in the DEGAS calculation increases the neutral density by a factor of between 1.5 and 4.0 in the private flux region, bringing the DEGAS results very close to the GTNEUT results and closer to the experimental results. The inclusion of molecules clearly makes a large contribution to the difference between the DEGAS and GTNEUT calculations of the neutral density in the private flux region. The DEGAS calculations that did not include molecules were generally in better agreement with the experiment, which also ignored molecular effects in calculating the neutral density from measured quantities, in the private flux region below the X point.

5.1.2. Wall boundary reflection differences

GTNEUT reflects incident neutral atoms from the wall and divertor plates as atoms at the incident

neutral temperature ($E_n = T_n$), which is assumed to be the ion temperature ($T_n = T_i$) of the region adjacent to the wall. These reflected atoms are isotropically distributed in direction. In DEGAS, a fraction of the incident neutrals is reflected as atoms, and the remainder is re-emitted as molecules. The fraction and the energy of the reflected/re-emitted neutrals depend on incident particle energy and material. Furthermore, particles are reflected with a cosine distribution for most wall material reflection models in DEGAS. The material used in the original DEGAS simulation shown in Fig. 9 was carbon. Thus, the Monte Carlo treatment of atoms and molecules reflected from a carbon wall is different from the isotropic reflection of atoms used by GTNEUT. The differences in both the angular distribution and the energy of reflected neutrals between the two codes could cause differences in the predicted neutral densities.

In order to understand the effect of this difference in the angular distribution of the reflected particles (cosine in DEGAS, isotropic in GTNEUT) two DEGAS simulations were performed. Both simulations were done without molecules and with $\langle\sigma\nu\rangle_{ion} \neq f(n)$, and differed only in the wall reflection condition. In the first simulation the wall material was carbon, which means the incident neutral atoms were reflected as cosine distributed atoms with an energy determined by the incident particle energy using the DEGAS surface physics model. In the second simulation the wall material acted as a mirror, which means that the incident particles were specularly reflected with the incident particle energy (effectively resulting in $E_n = T_n$). The mirror material option uses the same energy reflection condition as GTNEUT and would approximate, in regions with short mean free paths, the isotropic angular reflection condition used by the GTNEUT code (since particles would isotropize near the wall).

The Monte Carlo predictions indicated that the difference in angular distribution and/or energy of the reflected particles is important in the private flux region. The results for the calculation with a mirror wall were lower than the results of the calculation with the carbon wall by a factor of 2–5 below the X point in the private flux region. The difference between the two calculations in the core plasma was unimportant. It seems probable that the choice of wall reflection model could contribute to the difference seen in the predicted neutral densities in the private flux region between the Monte Carlo and GTNEUT results shown in Fig. 9.

5.2. DEGAS and GTNEUT benchmark

The results discussed above suggest that non-transport effects in the modelling of the experiment by DEGAS and GTNEUT could account, at least in large part, for the differences observed between DEGAS and GTNEUT in Fig. 9. We performed a final comparison between the two codes to determine the extent of these non-transport differences. For this purpose, two benchmark DEGAS models were constructed which modelled the atomic and molecular physics and the wall reflection conditions used in GTNEUT as closely as possible.

The first benchmark model used mirror wall reflection conditions (specular, $E_n = T_n$), no molecules and a density independent ionization rate. The mirror option was used in DEGAS to match the GTNEUT energy reflection condition ($E_n = T_n$) since in regions with short mean free path the reflected neutrals isotropize near the wall, creating an isotropic particle distribution similar to the isotropic reflection condition used by GTNEUT. The second DEGAS benchmark model used the carbon reflection condition, but without molecules. This second model, with a cosine angular distribution of reflected neutral atoms, is a closer match to the GTNEUT angular reflection conditions, but differs from GTNEUT in the energy of the reflected neutrals.

Since DEGAS does not allow different neutral temperatures at different locations with gas puffing, the particle source used in the Monte Carlo simulation was a neutral puff with a Maxwellian energy distribution characterized by the volume averaged ion temperature of the regions in front of the divertor plate. A similar energy distribution of puffed source particles was used in the GTNEUT calculations. DEGAS calculated the neutral energy distribution as a function of position, while GTNEUT used the local ion temperature approximation.

The results of this comparison are shown in Fig. 10. This figure also shows the original DEGAS calculation (which includes molecules and the carbon treatment of reflection) and the experimental measurements. The agreement between the GTNEUT (isotropic, $E_n = T_n$) and the first DEGAS (specular, $E_n = T_n$) benchmark calculation is remarkably good, both below and above the X point. The disagreement between the second DEGAS (cosine, $E_n \neq T_n$) benchmark calculation and GTNEUT (isotropic, $E_n = T_n$) is quite large.

From this we conclude that the differences in neutral densities between GTNEUT and DEGAS

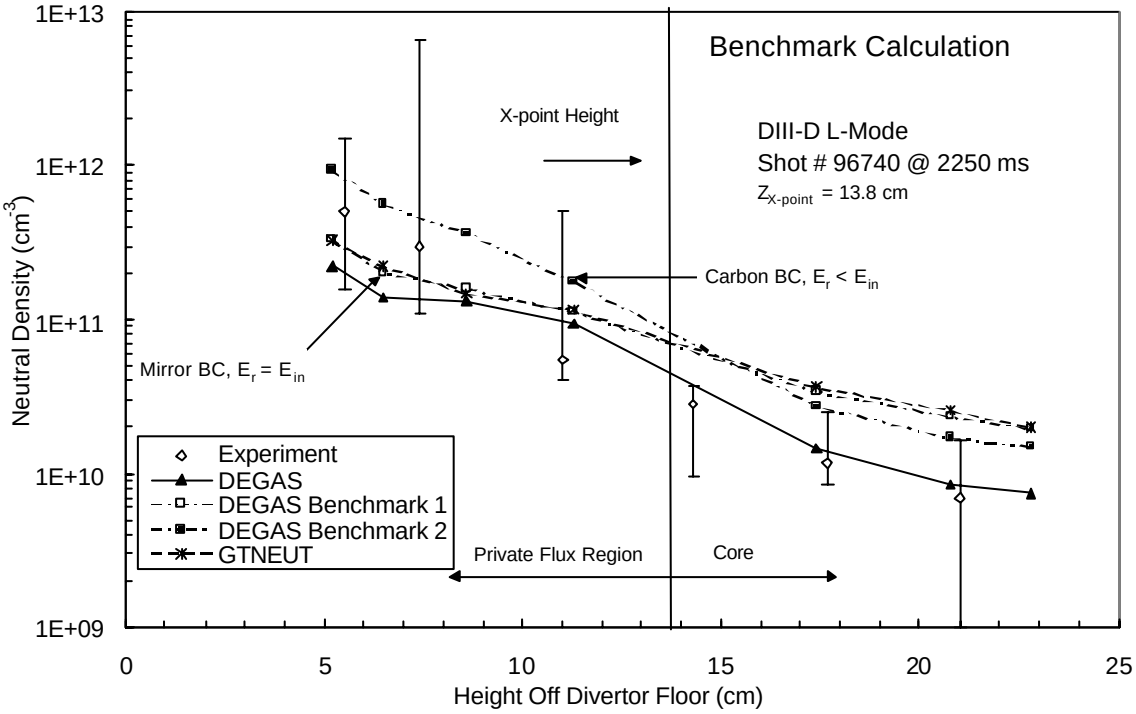

Figure 10. Benchmark calculation. GTNEUT (asterisks) and DEGAS (open squares) with gas puffing, mirror wall and no molecules; DEGAS (closed triangles) with particle recycling, carbon wall and molecules. DEGAS (closed squares) with gas puffing, carbon wall and no molecules.

arise principally from the inclusion of molecules in DEGAS and the treatment of the energy of the atoms reflected from the wall. When these two non-transport effects are eliminated, the agreement between the GTNEUT and DEGAS calculations is remarkably good.

6. Summary and conclusions

The accuracy of the assumptions made in the implementation of the TEP method has been evaluated by comparison of Monte Carlo and TEP calculations of simple model problems and of more complex models of present tokamaks, including an analysis of an experiment in which the neutral density was measured. This work has confirmed the promise of the TEP method by demonstrating that it can calculate neutral densities in rather good agreement with those predicted by Monte Carlo for the experimental configurations, at a small fraction (10^{-1}–10^{-3}) of the CPU time, while also identifying certain physics refinements that should be made to improve the accuracy of the existing TEP code, GTNEUT.

The four principal physics refinements that were identified are:

(a) Relaxation of the isotropic incident flux assumption, which can lead to underprediction of penetration;
(b) Relaxation of the non-directional escape probability assumption, which can lead to overprediction of penetration;
(c) Inclusion of molecules;
(d) Inclusion of a wall reflection model to calculate the energy of reflected atoms;
(e) Inclusion of volumetric recombination.

The most straightforward way to relax the isotropic incident flux (the DP_0 approximation) assumption is to extend the methodology to higher order DP_n expansions of the angular distribution, as has been done [16–23] in nuclear reactor physics applications of similar methods. The most promising way to relax the second potential limitation would seem to be by the development of first collision source corrections and directional escape probabilities. Molecular effects could be included either directly by adding ground and excited state molecular species to the

calculation or indirectly (and approximately) by calculating the number and energy of atoms formed by molecular dissociation in the region next to the recycling surface [24]. In addition to calculating the energy of atoms resulting from molecular dissociation, the energy of reflected atoms could be calculated from tables based on more detailed particle reflection codes such as TRIM.

Although not specifically identified as problems in this study, we plan two additional extensions of the TEP methodology presently implemented in GTNEUT. While our assumption that the neutrals in each region acquire a Maxwellian energy distribution with the local ion temperature was shown to be adequate in regions where the mean free path is comparable to the scale length of the temperature variation, it may be inadequate in regions near material walls or near vacuum regions. A multi-energy group approach could be adopted to provide a calculation of the neutral energy distribution. The inclusion of volumetric recombination is straightforward, since the TEP method is formulated with a volumetric source term.

Acknowledgements

This article is based on the PhD thesis [11] of the first author, in which a more detailed discussion can be found. The authors are grateful to R.J. Colchin, R. Maingi and L.W. Owen for providing information about the DIII-D neutrals measurements. This work was supported in part by the US Department of Energy under Grant No. DE-FG02-99-ER54538 with the Georgia Tech. Research Foundation.

References

[1] Niemczewski, A., et al., Nucl. Fusion **37** (1997) 151.
[2] Tsuchiya, K., et al., Plasma Phys. Control. Fusion **38** (1996) 1295.
[3] Stacey, W.M., Mahdavi, M.A., Maingi, R., Petrie, T.W., Phys. Plasmas **6** (1999) 3941.
[4] Stacey, W.M., Phys. Plasmas **4** (1997) 179.
[5] Stacey, W.M., Mandrekas, J., Nucl. Fusion **34** (1994) 1385.
[6] Stacey, W.M., Mandrekas, J., Rubilar, R., "Interface current integral transport methods for the calculation of neutral atom transport in the edge region of fusion plasmas", Fusion Technol. (in press).
[7] Wigner, E.P., Creutz, E., Jupnik, H., Snyder, T., Appl. Phys. **26** (1955) 260.
[8] Sauer, A., Nucl. Sci. Eng. **16** (1963) 260.
[9] Heifetz, D., Post, D., Petravic, D., Weisheit, J., Bateman, G., J. Comput. Phys. **46** (1982) 309.
[10] Stotler, D.P., Karney, C.F.F., Contrib. Plasma Phys. **34** (1994) 392.
[11] Rubilar, R., Neutral Particle Transport in the Plasma Edge and Divertor Region, PhD Thesis, Georgia Inst. of Technol., Atlanta (2000).
[12] Colchin, R.J., et al., Nucl. Fusion **40** (2000) 175.
[13] Colchin, R.J., Oak Ridge Natl Lab., TN, personal communication, 2000.
[14] Rensink, M.E., Lodestro, L., Porter, G.D., Rognlien, T.D., Contrib. Plasma Phys. **38** (1998) 325.
[15] Thomas, E.W., Stacey, W.M., Phys. Plasmas **4** (1997) 678.
[16] Anderson, M.M., Honeck, H.C., "An interface current technique for two-dimensional cell calculations", Mathematical Models and Computational Techniques for Analysis of Nuclear Systems (Proc. Conf. Ann Arbor, 1973), CONF-730414, Vol. 1, US Atomic Energy Commission (1973) 53.
[17] Sanchez, R., Nucl. Sci. Eng. **64** (1977) 384.
[18] Wasastjerna, F., Nucl. Sci. Eng. **72** (1979) 9.
[19] Krishnani, P.D., Ann. Nucl. Energy **10** (1985) 285.
[20] Sanchez, R., Nucl. Sci. Eng. **92** (1986) 247.
[21] Mohanakrishnan, P., Ann. Nucl. Energy **9** (1982) 261.
[22] Haggblom, H., Ahlin, A., Nucl. Sci. Eng. **56** (1975) 411.
[23] Chunlei, Z., Zhongsheng, X., Banghua, Y., Nucl. Sci. Eng. **100** (1988) 260.
[24] Stacey, W.M., Nucl. Fusion **40** (2000) 965.

(Manuscript received 26 September 2000
Final manuscript accepted 16 March 2001)

E-mail address of W.M. Stacey:
weston.stacey@me.gatech.edu

Subject classification: I1, Td; M0, Td